Article

The Impact of Retinal Configuration on the Protein-Chromophore Interactions in Bistable Jumping Spider Rhodopsin-1

Jonathan R. Church [1], Jógvan Magnus Haugaard Olsen[2] and Igor Schapiro[1,*]

[1] Fritz Haber Center for Molecular Dynamics Research Institute of Chemistry, The Hebrew University of Jerusalem, Jerusalem 9190401, Israel
[2] DTU Chemistry, Technical University of Denmark, DK-2800 Kgs. Lyngby, Denmark.
* Correspondence: Igor.Schapiro@mail.huji.ac.il

Abstract: Bistable rhodopsins have two stable forms which can be interconverted by light. Due to their ability to act as photoswitches, these proteins are considered as ideal candidates for applications such as optogenetics. In this work we analyze a recently crystalized bistable rhodopsin, namely the jumping spider rhodopsin-1 (JSR1). This rhodopsin exhibits identical absorption maxima for the parent and the photoproduct form, which impedes its broad application. We have performed hybrid QM/MM simulations to study three isomers of the retinal chromophore: the 9-*cis*, 11-*cis* and all-*trans* configurations. The main aim was to gain insight into the specific interactions of each isomer and their impact on the absorption maximum in JSR1. The absorption spectra were computed using sampled snapshots from a QM/MM molecular dynamics trajectory and compared to experimental counterparts. The chromophore-protein interactions were analyzed by visualizing the electrostatic potential of the protein and projecting it onto chromophore. It was found that the distance between a nearby tyrosine (Y126) residue plays a larger role in the predicted absorption maximum than the primary counterion (E194). Geometric differences between the isomers were also noted including a structural change in the polyene chain of the chromophore as well as changes in the nearby hydrogen bond network.

Keywords: Rhodopsins, Bistable, Jumping Spider, QM/MM, Spectral Tuning

1. Introduction

Rhodopsins constitute a family of photoreceptor proteins which share a common secondary structure of seven transmembrane helices.[1] These proteins gain their light sensitivity through an attached retinal (RET) chromophore that is covalently bound to the protein through a lysine residue. Together, lysine and RET form a retinal protonated Schiff base (RPSB) at their link. Rhodopsins can be further grouped into either monostable or bistable rhodopsins depending on the number of thermally stable intermediates in the photocycle of the protein. In the case of monostable rhodopsins, such as those found in bovine rhodopsin, the RPSB deprotonates along the photocycle. After the deprotonation event and a series of conformational changes of the protein, the Schiff base bond undergoes hydrolysis that ultimately leads to the release of the chromophore and bleaching of the sample.[2] In contrast, in bistable rhodopsins the photoproduct is thermally stable yielding a long-lived product which doesn't undergo bleaching. This characteristic of bistable rhodopsins is thought to be due to the RPSB remaining protonated throughout the photocycle.[3,4] This ability also elevates bistable rhodopsins as interesting candidates for optogenetics and other biotechnological applications, due to their ability to act as a photoswitch between the parent form and photoproduct.[5] Jumping spider rhodopsin-1 (JSR1) is such a bistable rhodopsin, first discovered within the jumping spider *Hasarius Adansoni* by Nagata and coworkers in 2012 (Fig 1.).[6] It also has the advantage of being a type II or animal rhodopsin which is supposedly better suited for optogenetics in mammalian cells.

Preprints (www.preprints.org) | NOT PEER-REVIEWED | Posted: 16 November 2021 doi:10.20944/preprints202111.0282.v1

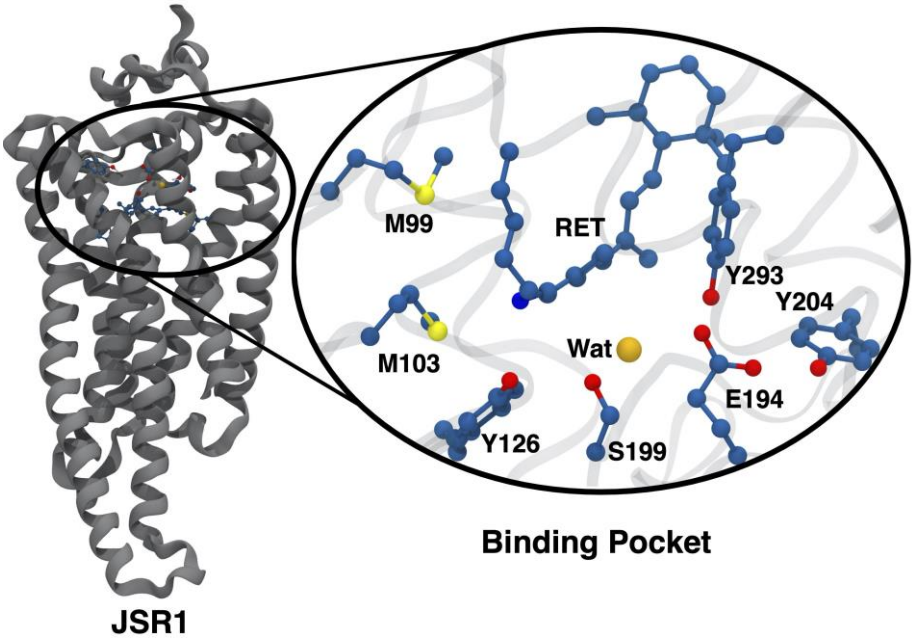

Figure 1. Crystal structure of jumping spider rhodopsin-1 (JSR1), containing the 9-*cis* form of retinal, taken from the protein data bank (PDB ID: 6I9K).[7] Also presented are several key residues in the retinal binding pocket. These include the counterion E194 and a crystallographic water thought to be important to the hydrogen bond network linking the RPSB.

The photocycle of JSR1 consists of a series of intermediates between the parent form (Rho) and an acid-Meta (a-Meta) photoproduct (Fig. 2).[2,3,5,8] Both forms of JSR1 can undergo photoisomerization induced by a photon. Rho isomerizes from 11-*cis* isomer of retinal (RET) to its all-*trans* form, and a-Meta undergoes the reverse reaction. However, the Rho and a-Meta forms have the same experimental absorption maxima at 535 nm.[2,9] The coinciding absorption maxima make the spectroscopic characterization difficult because the yield of each reaction is not unity and therefore a mixture of these two forms is obtained.[2]

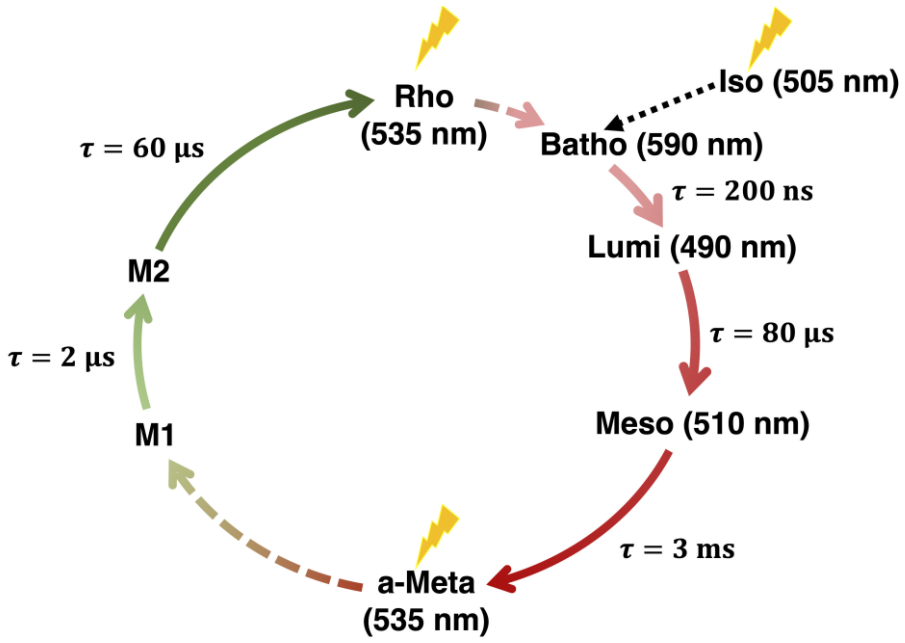

Figure 2. Photocycle of JSR1 showing the conversion between the Rho (11-*cis*) and a-Meta (all-*trans*) states as well as conversion of Iso (9-*cis*) to the Batho intermediate.

Preprints (www.preprints.org) | NOT PEER-REVIEWED | Posted: 16 November 2021 doi:10.20944/preprints202111.0282.v1

Initially, Nagata *et al.* have suggested that E194 is the counterion in JSR1, responsible for stabilization of the RPSB of both the parent and the photoproduct forms.[9] Unlike monostable rhodopsins where the RPSB has direct interactions with the nearby counterion, in JSR1 the E194 is too far for direct interactions with the RPSB (Fig. 1). The long separation between the counterion and RPSB implies that the charge of chromophore is stabilized through indirect interactions, such as an extended hydrogen bond network, although the exact mechanism is still unknown.[9] Mutational analysis in combination with pK_a studies by Nagata *et al.* suggest that the mechanism for the interaction between the RPSB and the local environment of the binding pocket is different for both the photoproduct and parent forms.[9] The serine in position 199 was targeted with several mutations including S199F, and S199A. Changes in this position were found to affect the pK_a and absorption maximum of the parent form to a much greater degree than that of the photoproduct. This suggests that there are different stabilizing mechanisms for the parent and photoproduct forms of JSR1. Similarly, mutations such as E194Q and E194D showed drastic changes to the absorption maximum for each isomer as well as the pK_a of the protonated Schiff base suggesting that this residue plays an important role in both the parent and photoproduct.[9]

Ehrenberg *et al.* characterized the photocycle of JSR1 using IR and UV/Vis spectroscopy of JSR1 reconstituted with the 9-*cis* RPSB.[2] This isomer exhibits a different absorption maximum from the 11-*cis* and all-*trans* chromophores. Following illumination, 9-*cis* isomerized to Batho and then forms a mixture of 11-*cis* and all-*trans* retinal chromophores due to the different lifetimes of these forms.[2] Ehrenberg *et al.* suggest that Rho to a-Meta are linked by three intermediates: Batho (τ=200ns, λ_{max}=590 nm), Lumi (τ=80μs, λ_{max}=490 nm) and Meso (τ=3ms, λ_{max}=510 nm). After forming a-Meta, an additional photon can be used to convert back to Rho which is thought to be linked by two intermediate states whose maximum absorbances were not directly observed, M1 (τ=2μs) and M2 (τ=60μs). Experimental evidence also suggests that Iso is linked to the traditional Rho/a-Meta photocycle through the Batho intermediate state (Fig. 2). Each isomer of retinal chromophore also exhibits unique FTIR and Raman spectra inside the protein environment that can be used to experimentally identify which isomer is bonded to the protein. Structural information of the chromophore itself can also be obtained from Raman data, where hydrogen-out-of-plane (HOOP) modes are shown to be low intensity for a-Meta relative to Rho, suggesting structural changes in the polyene chain of the chromophore upon formation of the photoproduct.[2] In this work we use the recently crystallized structure containing the 9-cis chromophore to model and investigate the effect that the 9-*cis*, 11-*cis* and all-*trans* isomers have on the local environment of the binding pocket in JSR1 using a combination of MM and hybrid QM/MM simulations.

2. Computational Methods

2.1 Model Generation

The crystal structure reported by Varma *et al.* (PDB ID: 6I9K) was used as the base structure for this study.[7] The 6I9K crystal structure is comprised of JSR1 with a bonded 9-*cis* RPSB. Missing loops were added using the Modeller program.[10] Due to the lack of crystal structures containing the 11-*cis* and all-*trans* isomers, the crystal structures of squid rhodopsin (SR) were used (PDB IDs: 2Z73[11] and 3AYM[12]) as a template for the orientation of the retinal chromophore. SR was already used to refine the crystal structure by Varma et al., due to their similar structural features including the hydrogen bonding network.[7] In this work the crystal structures of SR were used due to the structural similarity between JSR1 and SR, but more importantly due to the similarity in the binding pocket.[7] The peptide backbone of each these crystal structures were first aligned to that of 6I9K and the structures were generated by replacing the original 9-*cis* chromophore with the 11-*cis* and all-*trans* isomers. Each of the resulting structures were then embedded inside a bilayer of POPC lipid molecules using the CHARMM-GUI website.[13] The protonation

Preprints (www.preprints.org) | NOT PEER-REVIEWED | Posted: 16 November 2021 doi:10.20944/preprints202111.0282.v1

states of each titratable residue were further checked and assigned using the PROPKA3.0 program.[14,15]

2.2 Retinal Parameterization

Parameters for each isomer of the retinal chromophore were derived using the mdgx program found in AmberTools 16.[16] The bond, angle and dihedral parameters as well as the atomic RESP charges for each isomer were produced using gas-phase trajectories. Each isomer of the retinal chromophore was first optimized in the gas-phase using HF/6-31G*, the lysine link including the backbone atoms were kept and the severed peptide bonds were capped using hydrogens. Next, 30 initial conditions for each conformer in the gas-phase were generated using normal mode sampling where the energy of each normal mode was sampled using a Boltzmann distribution of energies at 300 K. The trajectories were then propagated using the GAMESS-US (2018, R3) program at the HF/6-31G* level of theory for 20 fs each using a timestep of 0.5 fs.[17] Snapshots were then generated using the resulting trajectory swarm every 1 fs and a RESP fitting was performed using the mdgx program in tandem with ORCA 4.2.0 at the HF/6-31G* level of theory.[18,19] This resulted in the fitting of 1260 snapshots for both the 11-*cis*/all-*trans* and 9-*cis*/all-*trans* parameter sets. During the fitting the point charges of the lysine link were fixed to that of a normal lysine, except for the epsilon carbon and its hydrogens. A restraint weight of 0.005 kcal/mol was placed on the charges of all heavy atoms of the chromophore when performing the RESP fitting. Equivalent hydrogens were also restrained to have the same value in the charge fitting. The RESP charges were then used to fit the bond, angle and dihedral parameters at the B3LYP/cc-pVTZ level of theory with the RIJCOSX approximation and D3 dispersion corrections, and with a tight SCF convergence criterion. The forcefield parameters were then iterated by optimizing the original set of snapshots with the mdgx program, together with the Amber program, which generated new structures and this process was repeated until the parameters had converged.

2.3 Classical and QM/MM Molecular Dynamics Simulations

The resulting crystal structures from the CHARMM-GUI website were minimized, heated and then classical dynamics were performed for 380 ns using the AMBER ff14SB forcefield for the protein and lipid14 for the POPC bilayer along with our derived chromophore parameters for the retinal chromophores.[20,21] The 9-*cis*/all-*trans* parameter set was used for both the 9-*cis* and all-*trans* models. SHAKE was used to constrain the motion of the bonds involving hydrogen unless otherwise noted. First, each model was minimized using the classical force field for 100,000 steps. During the minimization a restraint weight of 10 kcal/mol was placed on all atoms including hydrogens. A thermal equilibration step was then performed by heating the models from 0 to 300 K at constant volume and temperature for 500 ps using a timestep of 1 fs with constraints placed on heavy and light atoms as outlined in the supporting information (Table S1). Next, six separate steps of equilibration were performed for 250 ps each at a constant pressure of 1 atm and temperature of 300 K while the restraints were slowly released (See methodology). After releasing all restraints, a run was performed for 300 ns at constant pressure and temperature with a 2 fs timestep. Finally, SHAKE was removed from the protein and an additional 80 ns equilibration step was performed with a timestep of 1 fs. To generate snapshots for spectra generation additional QM/MM MD trajectories were produced by continuing the aforementioned MM trajectories using the DFTB2+D method found within Amber with an electrostatic embedding scheme.[16] The QM region was defined as the retinal chromophore and lysine link cut between the C_β-C_α bond and capped with a hydrogen atom to exclude the peptide backbone. The MM partition included the remaining protein, lipids, ions and waters that were treated with the classical ff14SB Amber forcefield with a

 doi:10.20944/preprints202111.0282.v1

12 Å non-bonding cutoff.[20] DFTB was chosen to treat the QM region because this method has been shown to yield structures in close agreement with those obtained using the B3LYP functional with medium sized basis sets while still remaining computationally feasible for trajectories in the nanosecond time-scale.[22–24] These QM/MM trajectories were propogated for 1 ns with a timestep of 1 fs at 300 K using the Langevin thermostat and keeping the pressure at 1 atm. Additionally SHAKE was not used for hydrogens of the protein. The resulting QM/MM trajectories were then used to generate snapshots for spectra generation of each model by taking a snapshot of the trajectory every 10 ps resulting in 100 snapshots.[25]

2.4 Spectra Generation

The excitation energies were determined with time-dependent density functional theory (TD-DFT) using the CAM-B3LYP functional and cc-pVDZ basis. [26,27] The TD-DFT excitation energies of each snapshot were determined for the lowest 10 excited states using electrostatic embedding. The QM region consisted of the chromophore and the lysine sidechain, which was capped with a hydrogen link atom. The TD-CAM-B3LYP calculations were performed using the Dalton program.[28,29] The protein, lipids, ions and solvent in the calculations were described using point charges from the ff14SB and lipid14 forcefields with a 50 Å cutoff from the RET residue. Each set of resulting stick spectra were then broadened assuming a Gaussian band shape and the final spectra were determined by averaging over the 100 conformations at each wavelength.

3. Results and Discussion

3.1. Structural Differences between the Isomers

Analysis of the resulting QM/MM MD trajectories for the 9-*cis*, 11-*cis* and all-*trans* RPSB isomers showed several structural differences in the arrangement of the binding pocket (Fig. 4). The average structure of each isomer was calculated from the trajectories and visualized to analyze any differences caused by configuration of the chromophore (Fig. 4 B-C). The 9-*cis* and 11-*cis* models were found to each contain a water linking E194 and S199 through hydrogen bonds (Fig. 4 B, C). This water has been suggested to participate in the hydrogen bonding network, linking the distant E194 to the RPSB for Rho of JSR1.[9] In the case of the all-*trans* chromophore, the polyene chain of chromophore twists in such a way that a methyl group at C_{13} occupies the water position found in the 9-*cis* and 11-*cis* structures, leading to a loss of the water between E194 and S199. The loss of this water causes the direct interaction of E194 counterion with that of S199 (Fig. 4 D). The change in the polyene chain is consistent with the Raman spectra analysis performed by Ehrenberg et al. who reported that the intensity of HOOP modes belonging to the retinal chromophore change upon isomerization between 11-*cis* and all-*trans* isomers indicating a distorted polyene chain in 11-*cis*.[2] These QM/MM trajectories were also analyzed by Ricardi et al. who studied how clustering the chromophores into several average structures impacted the predicted excitation energies. These authors found that the primary structural changes in the chromophore over the 1 ns trajectories were due to conformational changes in both the lysine link and β-ionone ring.[30] The 9-*cis* chromophore was found to have the greatest movement of the lysine chain, and each isomer the showed two configurations of the β-ionone ring. The increased movement of the lysine chain is reflected in the average orientation of 9-*cis* lysine link in comparison to 11-*cis* and all-*trans*, which are roughly the same.

Preprints (www.preprints.org) | NOT PEER-REVIEWED | Posted: 16 November 2021 doi:10.20944/preprints202111.0282.v1

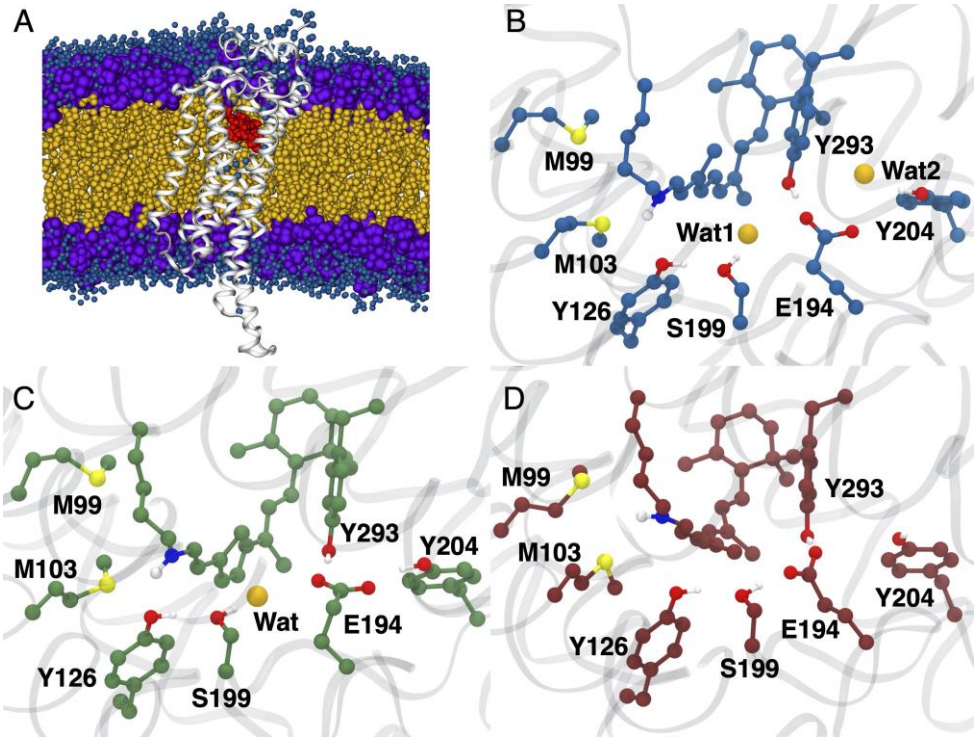

Figure 3. A) JSR1 protein in a membrane following the production procedure outlined in the methodology, along with the chromophore in red and nearby waters represented as blue spheres. B-D) show the 9-*cis*, 11-*cis* and all-*trans* RPSB with key residues in the binding pocket.

To quantify the amount of water located near the retinal chromophore over the 1 ns QM/MM MD trajectory, the integrated radial distribution function (RDF) was determined for each isomer (Fig. 4). The integrated RDF of each isomer shows that over the course of the QM/MM MD trajectory there were more waters in close proximity to the 9-*cis*/11-*cis* chromophores than to the all-*trans* isomer, which is consistent with the average structures (Fig. 3B-D).[9]

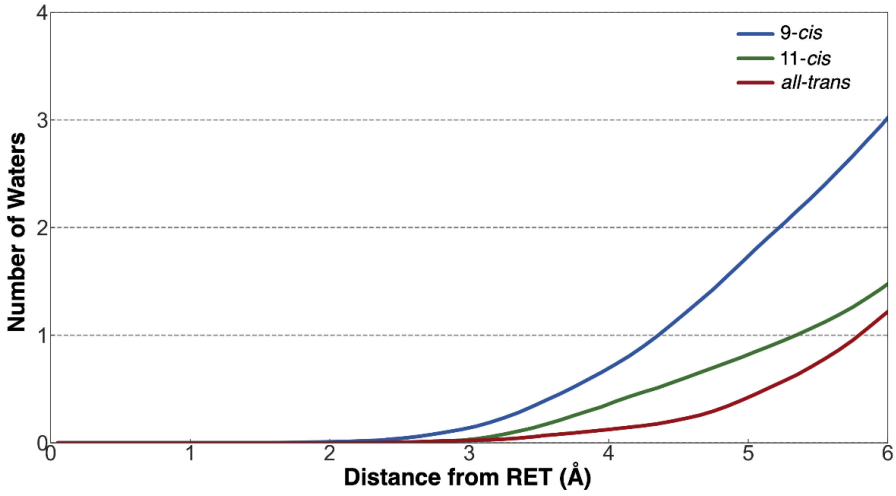

Figure 4. Integrated radial distribution function of waters from chromophore using the 1 ns QM/MM MD trajectories.

In the all-*trans* model, the methyl functional group pushes a water out of the binding pocket and away from polyene chain due to a twist. Interestingly, the water linking residues E194 and S199 in the 11-*cis* model is found to be positioned slightly further away than that of the 9-cis model. The counterion itself is stabilized by residues Y185/Y274,

Preprints (www.preprints.org) | NOT PEER-REVIEWED | Posted: 16 November 2021 doi:10.20944/preprints202111.0282.v1

whereas in the 9-cis model, the E194 counterion is stabilized by an additional water found in close proximity to Y185.

3.2. Changes in the Electrostatic Environment

Electrostatic potential maps of the protein environment were generated for the average structure of each isomer model. These maps were then projected onto the van der Waals surface of the corresponding retinal chromophore to visualize the changes of the environment and how it impacts the protein-chromophore interactions (Fig. 5).

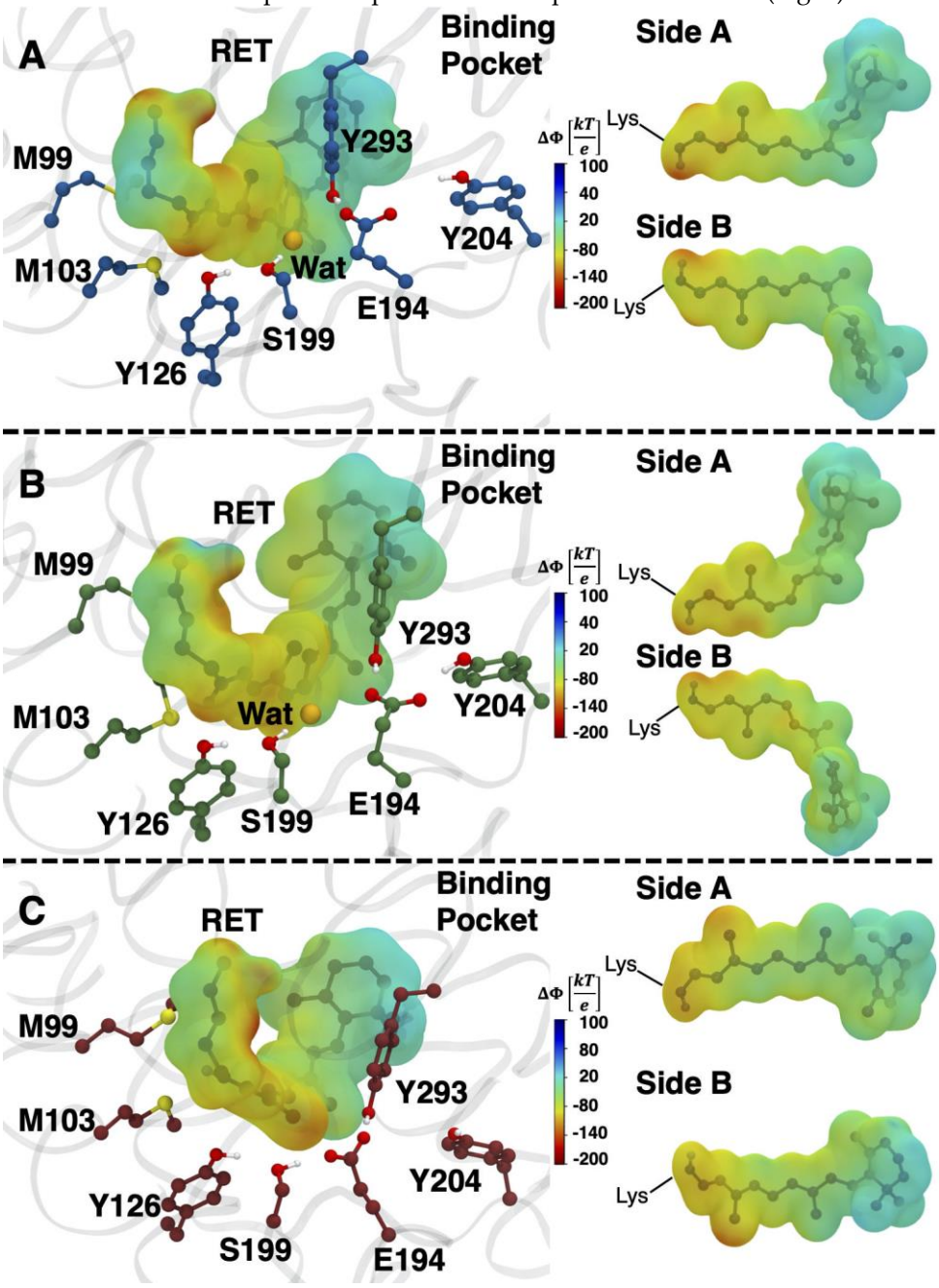

Figure 5. Electrostatic potentials generated for the **(A)** 9-*cis*, **(B)** 11-*cis* and **(C)** all-*trans* models determined using APBS[31] and VMD[32]. The electrostatic interactions between the chromophore and the full protein environment were examined. Red indicates a negative electrostatic interaction from the environment and blue indicates a positive electrostatic interaction. Also shown are side views of the retinal chromophore excluding the lysine sidechain except for the Schiff base nitrogen.

 doi:10.20944/preprints202111.0282.v1

The electrostatic potentials show that the 9-*cis* model has a more negative interaction near the RPSB (see side views of the chromophore in Fig 5A). It appears that the negative electrostatic interaction with Y126 stabilizes the positively charged Schiff base. However, the structural changes of the polyene chain in the all-*trans* model limit the direct interactions of the RPSB with Y126, which instead has a preferential interaction with M99 and M103. This finding is supported by the analysis of the hydrogen bonding partners of the RPSB over the QM/MM MD trajectory. The analysis shows that the Schiff base region of the 9-*cis*, 11-*cis* and all-*trans* models interacted with M103 39.4%, 39.2%, and 24.9% of the trajectory, respectively. In addition, the nearby M99 residue is hydrogen bonded to the Schiff base for 18.3% of the snapshots of all-*trans*, but 0% for either *cis* isomer. Both the 9-*cis* and 11-*cis* models interact directly with Y126 for 23.0% and 6.2% of the trajectory, respectively. The E194 counterion does not seem to function as the primary cause of stabilizing interaction in any of the models, because its average distance to the Schiff base, measured as N15 (RET)···O (E194) separation was 6.95 Å, 6.49 Å and 6.12 Å for the 9-*cis*, 11-*cis* and all-*trans* chromophores, respectively. Therefore, Y126 proximity to the Schiff base appears to play a much larger role in the chromophore-protein interactions where the average N15 (RET)···O (Y126) distance was 3.04 Å, 3.14 Å and 3.72 Å. This is reflected in the visualization of the electrostatic potentials (Fig. 5) that show the enhanced negative electrostatic interaction in the Schiff base region of the 9-*cis* and 11-*cis* structures occurs near Y126.

3.3. Absorption Maxima

The absorption spectra of the isomers were generated from 100 structures taken from the 1 ns QM/MM MD trajectories and using TD-CAM-B3LYP with the cc-pVDZ basis (Fig. 6 A,B and Table 1). The calculated absorption maxima were 2.56 eV, 2.42 eV and 2.40 eV for the 9-*cis*, 11-*cis* and all-*trans* chromophores, respectively (Fig. 6A). The absorption maxima are blue shifted by 0.1 eV relative to their experimental counterpart, well within the normal deviation produced from using TD-DFT methods to calculate vertical excitation energies.[33–36] The relative shifts between the absorption maxima of each isomer (Fig. 6C) were also in good agreement with experimental values with an error of 0.02 eV or less. Determining the absorption maximum of each isomer in vacuum (Fig. 6B) red-shifted the absorption maxima. Both 11-*cis* and all-*trans* were found to be less sensitive to this effect, red-shifting by 0.11 eV and 0.10 eV, in comparison to the 9-*cis* which red-shifted by 0.18 eV.

Preprints (www.preprints.org) | NOT PEER-REVIEWED | Posted: 16 November 2021 doi:10.20944/preprints202111.0282.v1

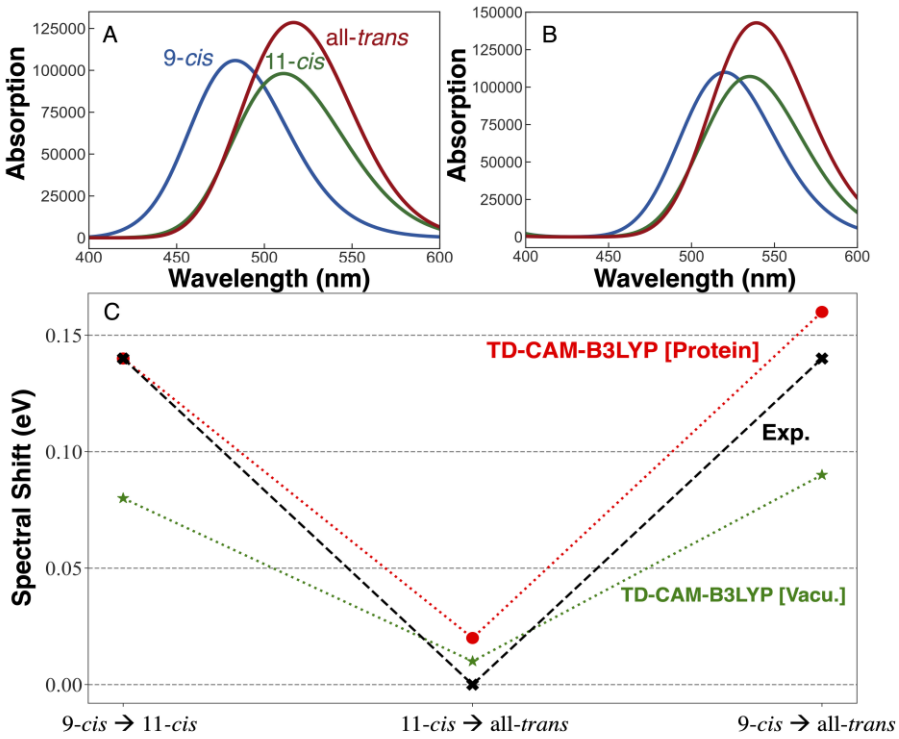

Figure 6. Absorption maxima of the three models determined from 100 snapshots taken from the DFTB2+D trajectories. The excitation energies of these snapshots were calculated using TD-CAM-B3LYP/cc-pVDZ **(A)** in the protein environment and **(B)** in the gas-phase. Also shown **(C)** are the relative shifts between the absorption maxima of the three models for comparison to experimental shifts from Ehrenberg.[2]

Table 1. Absorption maximum of each isomer in vacuum and in protein modeled using electrostatic embedding as well as the experimental values.[2,7]

	Vacuum (nm, eV)	TD-CAM-B3LYP (nm, eV)	Exp. (nm, eV) [2,7]
9-cis	520, 2.38	484, 2.56	505, 2.46
11-cis	537, 2.31	512, 2.42	535, 2.32
all-trans	540, 2.30	517, 2.40	535, 2.32

Spectral tuning in rhodopsins is often explained using the external point charge model developed by Honig and coworkers.[37–40] This model is based on evidence showing that the S_1-S_0 excitation in gas-phase RPSB is accompanied by a transfer of the positive charge of the Schiff base moiety towards the β-ionone ring (Fig. 8). Placing a negatively charged residue at either end of chromophore can affect the stability of the ground (S_0) and excited states (S_1), and ultimately create a shift in the absorption maximum.

Preprints (www.preprints.org) | NOT PEER-REVIEWED | Posted: 16 November 2021 doi:10.20944/preprints202111.0282.v1

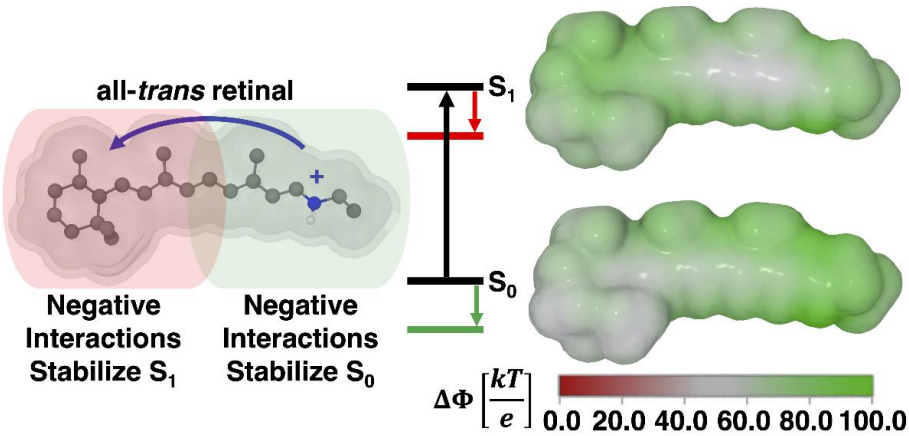

Figure 7. Point charge model schematic for the gas-phase all-*trans* retinal chromophore. Here the electrostatic potential (**ΔΦ**) shows positive charge as a green color. The schematic shows that the positive charge in the ground state (S_0) is localized near the Schiff base. Upon excitation to S_1 a partial charge moves towards the β-ionone ring.

In our work, the 9-*cis* isomer experienced a larger stabilization of the RPSB by the protein (Fig. 6) and thus embedding this chromophore in the protein environment produced a greater blue-shift of the absorption maximum. In comparison, the all-*trans* and 11-*cis* isomers had roughly the same amount of stabilization of the Schiff base upon being embedded in the protein environment, which helps explain why these models exhibit roughly the same absorption maxima (Table 1) and why moving from vacuum to protein produced a much larger shift for 9-*cis* (0.18 eV) in comparison to 11-cis (0.11 eV) and all-*trans* (0.10 eV).

4. Conclusion

The spectral shift between the 9-*cis* and 11-*cis*/all-*trans* isomers of the retinal chromophore in JSR1 appear to be controlled by the proximity of a nearby Y126 residue to the RPSB rather than the E194 counterion. The 9-*cis* chromophore is closest to Y126 and has more hydrogen bonding interactions and in turn experiences a larger blue-shift of the absorption maximum upon inclusion of the protein environment. This is supported by the electrostatic potential maps of each isomer which shows that the 9-*cis* chromophore has a large negative interaction with the environment near the location of the Y126 residue. Similarly, the distance of the E194 counterion to the Schiff base indicates that it does not appear to have a direct effect on the predicted absorption maxima. There were also key geometric changes found in the models, where the polyene chain of the all-*trans* chromophore twisted in such a way that limited the RPSB from interacting with Y126 and which instead interacted with M103/M99 as hydrogen bonding partners. These findings are in agreement with the Raman spectroscopic results of Ehrenberg et al. who noticed that HOOP modes predict a different polyene chain orientation between 11-*cis* and all-*trans*. The results of our findings may be used to help explain the stability of JSR1 and other bistable rhodopsins as well as help guide experimentalists hoping to use these types of proteins as photoswitches for optogenetics.

Supplementary Materials: The following are available online at www.mdpi.com/xxx/s1, Table S1: Constraints (kcal/mol·Å²) used during each step of dynamics with Amber.

Author Contributions I.S. initially conceived this project and acted in a supervising role. J.R.C. generated the models and parameters used in this study as well as performed the dynamical simulations. J.M.H.O and J.R.C. were responsible for obtaining the data used in spectra generation. J.R.C. wrote the initial draft of the paper, and all authors contributed to discussions and editing of the final draft.

Funding: I.S. thanks the DFG Collaborative Research Center 1078, project C6 for support. I.S. gratefully acknowledges funding by the European Research Council (ERC) under the European Union's Horizon 2020 research and innovation program (Grant No. 678169 "PhotoMutant"). J.R.C thanks the Zuckerman STEM Leadership Program for their support. J.M.H.O. thanks VILLUM FONDEN for financial support (grant no. 29478).

Conflicts of Interest: The authors declare no conflict of interest.

References

1. Palczewski, K. G protein-coupled receptor rhodopsin. *Annu. Rev. Biochem.* 2006, *75*, 743–767.
2. Ehrenberg, D.; Varma, N.; Deupi, X.; Koyanagi, M.; Terakita, A.; Schertler, G.F.X.; Heberle, J.; Lesca, E. The Two-Photon Reversible Reaction of the Bistable Jumping Spider Rhodopsin-1. *Biophys. J.* **2019**, *116*, 1248–1258, doi:10.1016/j.bpj.2019.02.025.
3. Li, B.; Vachali, P.; Bernstein, P.S.; Photobiol Sci, P.; Tsutsui, K.; Shichida, Y.; Tsukamoto, H.; Terakita, A.; Davies, W.L.; Hankins, M.W.; et al. Diversity and functional properties of bistable pigments. *Photochem. Photobiol. Sci.* **2010**, *9*, 1435–1443, doi:10.1039/C0PP00168F.
4. HUBBARD, R.; ST GEORGE, R.C. THE RHODOPSIN SYSTEM OF THE SQUID. *J. Gen. Physiol.* **1958**, *41*, 501, doi:10.1085/JGP.41.3.501.
5. Koyanagi, M.; Terakita, A. Diversity of animal opsin-based pigments and their optogenetic potential. *Biochim. Biophys. Acta - Bioenerg.* **2014**, *1837*, 710–716, doi:10.1016/J.BBABIO.2013.09.003.
6. Nagata, T.; Koyanagi, M.; Tsukamoto, H.; Saeki, S.; Isono, K.; Shichida, Y.; Tokunaga, F.; Kinoshita, M.; Arikawa, K.; Terakita, A. Depth Perception from Image Defocus in a Jumping Spider. *Science (80-.).* **2012**, *335*, 469–471, doi:10.1126/SCIENCE.1211667.
7. Varma, N.; Mutt, E.; Mühle, J.; Panneels, V.; Terakita, A.; Deupi, X.; Nogly, P.; Schertler, G.F.X.; Lesca, E. Crystal structure of jumping spider rhodopsin-1 as a light sensitive GPCR. *Proc. Natl. Acad. Sci. U. S. A.* **2019**, *116*, 14547–14556, doi:10.1073/pnas.1902192116.
8. Matsuyama, T.; Yamashita, T.; Imamoto, Y.; Shichida, Y. Photochemical properties of mammalian melanopsin. *Biochemistry* **2012**, *51*, 5454–5462, doi:10.1021/BI3004999/SUPPL_FILE/BI3004999_SI_002.PDF.
9. Nagata, T.; Koyanagi, M.; Tsukamoto, H.; Mutt, E.; Schertler, G.F.X.; Deupi, X.; Terakita, A. The counterion–retinylidene Schiff base interaction of an invertebrate rhodopsin rearranges upon light activation. *Commun. Biol.* **2019**, *2*, 1–9, doi:10.1038/s42003-019-0409-3.
10. Šali, A.; Blundell, T.L. Comparative protein modelling by satisfaction of spatial restraints. *J. Mol. Biol.* **1993**, *234*, 779–815, doi:10.1006/jmbi.1993.1626.
11. Murakami, M.; Kouyama, T. Crystal structure of squid rhodopsin. *Nat. 2008 4537193* **2008**, *453*, 363–367, doi:10.1038/nature06925.
12. Murakami, M.; Kouyama, T. Crystallographic Analysis of the Primary Photochemical Reaction of Squid Rhodopsin. *J. Mol. Biol.* **2011**, *413*, 615–627, doi:10.1016/J.JMB.2011.08.044.
13. Jo, S.; Kim, T.; Iyer, V.G.; Im, W. CHARMM-GUI: A web-based graphical user interface for CHARMM. *J. Comput. Chem.* **2008**, *29*, 1859–1865, doi:10.1002/JCC.20945.
14. Olsson, M.H.M.M.; Søndergaard, C.R.; Rostkowski, M.; Jensen, J.H. PROPKA3: Consistent treatment of internal and surface residues in empirical p K a predictions. *J. Chem. Theory Comput.* **2011**, *7*, 525–537, doi:10.1021/ct100578z.
15. Søndergaard, C.R.; Olsson, M.H.M.; Rostkowski, M.; Jensen, J.H. Improved Treatment of Ligands and Coupling Effects in Empirical Calculation and Rationalization of pKa Values. *J. Chem. Theory Comput.* **2011**, *7*, 2284–2295, doi:10.1021/CT200133Y.
16. Case, D.A.; Cheatham, T.E.; Darden, T.; Gohlke, H.; Luo, R.; Merz, K.M.; Onufriev, A.; Simmerling, C.; Wang, B.; Woods, R.J. The Amber biomolecular simulation programs. *J. Comput. Chem.* 2005, *26*, 1668–1688.
17. Schmidt, M.W.; Baldridge, K.K.; Boatz, J.A.; Elbert, S.T.; Gordon, M.S.; Jensen, J.H.; Koseki, S.; Matsunaga, N.; Nguyen, K.A.; Su, S.; et al. General atomic and molecular electronic structure system. *J. Comput. Chem.* **1993**, *14*, 1347–1363,

doi:10.1002/jcc.540141112.

18. Debiec, K.T.; Cerutti, D.S.; Baker, L.R.; Gronenborn, A.M.; Case, D.A.; Chong, L.T. Further along the Road Less Traveled: AMBER ff15ipq, an Original Protein Force Field Built on a Self-Consistent Physical Model. *J. Chem. Theory Comput.* **2016**, *12*, 3926–3947, doi:10.1021/acs.jctc.6b00567.
19. Neese, F. Software update: the ORCA program system, version 4.0. **2018**, *8*, e1327.
20. Maier, J.A.; Martinez, C.; Kasavajhala, K.; Wickstrom, L.; Hauser, K.E.; Simmerling, C. ff14SB: Improving the Accuracy of Protein Side Chain and Backbone Parameters from ff99SB. *J. Chem. Theory Comput.* **2015**, *11*, 3696–3713.
21. Dickson, C.J.; Madej, B.D.; Skjevik, Å.A.; Betz, R.M.; Teigen, K.; Gould, I.R.; Walker, R.C. Lipid14: The amber lipid force field. *J. Chem. Theory Comput.* **2014**, *10*, 865–879, doi:10.1021/CT4010307/SUPPL_FILE/CT4010307_SI_001.PDF.
22. Adam, S.; Bondar, A.N. Mechanism by which water and protein electrostatic interactions control proton transfer at the active site of channelrhodopsin. *PLoS One* **2018**, *13*, e0201298, doi:10.1371/JOURNAL.PONE.0201298.
23. Gaus, M.; Cui, Q.; Elstner, M. DFTB3: Extension of the self-consistent-charge density-functional tight-binding method (SCC-DFTB). *J. Chem. Theory Comput.* **2011**, *7*, 931–948, doi:10.1021/CT100684S/SUPPL_FILE/CT100684S_SI_002.XLS.
24. Adam, S.; Wiebeler, C.; Schapiro, I. Structural Factors Determining the Absorption Spectrum of Channelrhodopsins: A Case Study of the Chimera C1C2. **2020**, doi:10.26434/CHEMRXIV.12400676.V1.
25. Seabra, G.D.M.; Walker, R.C.; Elstner, M.; Case, D.A.; Roitberg, A.E. Implementation of the SCC-DFTB Method for Hybrid QM/MM Simulations within the Amber Molecular Dynamics Package †. *ACS Publ.* **2007**, *111*, 5655–5664, doi:10.1021/jp0700711.
26. Runge, E.; Gross, E.K.U. Density-functional theory for time-dependent systems. *Phys. Rev. Lett.* **1984**, *52*, 997–1000, doi:10.1103/PhysRevLett.52.997.
27. Hättig, C. Structure Optimizations for Excited States with Correlated Second-Order Methods: CC2 and ADC(2). *Adv. Quantum Chem.* 2005, *50*, 37–60.
28. Olsen, J.M.H.; Reine, S.; Vahtras, O.; Kjellgren, E.; Reinholdt, P.; Hjorth Dundas, K.O.; Li, X.; Cukras, J.; Ringholm, M.; Hedegård, E.D.; et al. Dalton Project: A Python platform for molecular- and electronic-structure simulations of complex systems. *J. Chem. Phys.* **2020**, *152*, 214115, doi:10.1063/1.5144298.
29. Aidas, K.; Angeli, C.; Bak, K.L.; Bakken, V.; Bast, R.; Boman, L.; Christiansen, O.; Cimiraglia, R.; Coriani, S.; Dahle, P.; et al. The Dalton quantum chemistry program system. *Wiley Interdiscip. Rev. Comput. Mol. Sci.* **2014**, *4*, 269–284, doi:10.1002/wcms.1172.
30. Ricardi, N.; González-Espinoza, C.E.; Adam, S.; Church, J.; Schapiro, I.; Wesolowski, T.A. Embedding non-rigid solutes in an averaged environment: a case study on rhodopsins. **2021**, doi:10.26434/CHEMRXIV-2021-86W18.
31. Jurrus, E.; Engel, D.; Star, K.; Monson, K.; Brandi, J.; Felberg, L.E.; Brookes, D.H.; Wilson, L.; Chen, J.; Liles, K.; et al. Improvements to the APBS biomolecular solvation software suite. *Protein Sci.* **2018**, *27*, 112–128, doi:10.1002/pro.3280.
32. Humphrey, W.; Dalke, A.; Schulten, K. VMD: Visual molecular dynamics. *J. Mol. Graph.* **1996**, *14*, 33–38, doi:10.1016/0263-7855(96)00018-5.
33. Chibani, S.; Jacquemin, D.; Laurent, A.D. Modelling solvent effects on the absorption and emission spectra of constrained cyanines with both implicit and explicit QM/EFP models. *Comput. Theor. Chem.* **2014**, *1040–1041*, 321–327, doi:10.1016/J.COMPTC.2014.03.033.
34. Ziegler, T.; Krykunov, M.; Cullen, J. The implementation of a self-consistent constricted variational density functional theory for the description of excited states. *J. Chem. Phys.* **2012**, *136*, 124107, doi:10.1063/1.3696967.
35. Demoulin, B.; El-Tahawy, M.M.T.; Nenov, A.; Garavelli, M.; Le Bahers, T. Intramolecular photo-induced charge transfer in visual retinal chromophore mimics: electron density-based indices at the TD-DFT and post-HF levels. *Theor. Chem. Acc.* **2016**, *135*, 1–10, doi:10.1007/S00214-016-1815-Y/FIGURES/12.
36. Fujimoto, K.; Hayashi, S.; Hasegawa, J.Y.; Nakatsuji, H. Theoretical studies on the color-tuning mechanism in retinal proteins.

J. Chem. Theory Comput. **2007**, *3*, 605–618, doi:10.1021/CT6002687/SUPPL_FILE/CT6002687-FILE001.PDF.

37. Motto, M.G.; Sheves, M.; Tsujimoto, K.; Balogh-Nair, V.; Nakanishi, K. Opsin Shifts in Bovine Rhodopsin and Bacteriorhodopsin. Comparison of Two External Point-Charge Models. *J. Am. Chem. Soc.* **1980**, *102*, 7947–7949, doi:10.1021/JA00547A029.
38. Nakanishi, K.; Balogh-Nair, V.; Amaboldi, M.; Tsujimoto, K.; Honig, B. An External Point-Charge Model for Bacteriorhodopsin To Account for Its Purple Color. *J. Am. Chem. Soc.* **1980**, *102*, 7945–7947, doi:10.1021/JA00547A028.
39. Barry, H.; Uri, D.; Koji, N.; Valeria, B.N.; Gawinowicz, M.A.; Maria, A.; Motto, M.G. An External Point-Charge Model for Wavelength Regulation in Visual Pigments. *J. Am. Chem. Soc.* **1979**, *101*, 7084–7086, doi:10.1021/JA00517A060.
40. Mordechai, S.; Koji, N.; Barry, H. Through-Space Electrostatic Effects in Electronic Spectra. Experimental Evidence for the External Point-Charge Model of Visual Pigments. *J. Am. Chem. Soc.* **1979**, *101*, 7086–7088, doi:10.1021/JA00517A061.